Chemical Physics Letters 732 (2019) 136649

Contents lists available at ScienceDirect

Chemical Physics Letters

journal homepage: www.elsevier.com/locate/cplett

Research paper

Strain and electric field engineering of band alignment in InSe/$Ca(OH)_2$ heterostructure

Khang D. Pham[a,b], Trinh D. Nguyen[c], Huynh V. Phuc[d], Nguyen N. Hieu[e], H.D. Bui[e,*], Bin Amin[f], Chuong V. Nguyen[g,*]

[a] Laboratory of Applied Physics, Advanced Institute of Materials Science, Ton Duc Thang University, Ho Chi Minh City, Viet Nam
[b] Faculty of Applied Sciences, Ton Duc Thang University, Ho Chi Minh City, Viet Nam
[c] NTT Hi-Tech Institute, Nguyen Tat Thanh University, Ho Chi Minh City, Viet Nam
[d] Division of Theoretical Physics, Dong Thap University, Cao Lanh 870000, Viet Nam
[e] Institute of Research and Development, Duy Tan University, Da Nang 550000, Viet Nam
[f] Department of Physics, Abbottabad University of Science and Technology, Abbottabad, Pakistan
[g] Department of Materials Science and Engineering, Le Quy Don Technical University, Ha Noi, Viet Nam

HIGHLIGHTS

- Structural and electronic properties of combined InSe/$Ca(OH)_2$ heterostructures were investigated through DFT calculations.
- Combination of InSe and $Ca(OH)_2$ tends to a significant decrease in the band gap of heterostructure.
- InSe/$Ca(OH)_2$ heterostructure mediates by the weak vdW interactions and possesses a type-II semiconductor.
- Type-II band alignment of heterostructure can be engineered by applying electric field or vertical strains.
- Semiconductor-to-metal and direct-to-indirect transitions can be emerged, which make InSe/$Ca(OH)_2$ heterostructure promising material.

ARTICLE INFO

Keywords:
DFT calculations
van der Waals heterostructures
Band gap controllable
Strain engineering
Electric field

ABSTRACT

In this work, we investigate the structural and electronic properties of the combined InSe/$Ca(OH)_2$ heterostructure through density functional theory. It suggests that a combination of InSe and $Ca(OH)_2$ tends to a significant decrease in the band gap of the heterostructure, which may result from the vacuum energy difference of the monolayers. The InSe/$Ca(OH)_2$ heterostructure mediates by the weak vdW interactions and possesses a type-II semiconductor with a direct band gap of 0.55 eV, which can also be engineered by applying electric field or vertical strains. The semiconductor-to-metal and direct-to-indirect transitions can also emerge, which make InSe/$Ca(OH)_2$ heterostructure promising material for electronic nanodevices.

1. Introduction

Following the successful synthesis of graphene in 2004 by Geim et al. [1], various novel two-dimensional (2D) materials with desirable physical and chemical properties for future high-performance applications have been successfully synthesized experimentally [2–9]. Owing to their great properties, these 2D materials are highly desirable for use in novel electronic and optoelectronic applications. Besides the great above-mentioned properties, single layered 2D materials are still disadvantages, that may affect their applicability in high-frequency components. For example, the absence of an electronic band gap in graphene has hindered its application in logic nanodevices. Whereas, the low intrinsic carrier mobility of MoS_2 monolayer of about 200 cm^2/Vs has limited its application in high-speed nanodevices. Recently, there exist many strategies to control the electronic and transport properties of 2D materials, such as strain engineering [10], doping [11–14], functionalization, electric and magnetic fields [15–19]. Especially, a new strategy in materials science has currently come on the scene that relates to the vertical stacking of two or more different single-layered 2D materials on top of each other, namely, van der Waals heterostructures (vdW-HTSs). Such a combination can be used to increase the application range of 2D materials towards electronic and optoelectronic nanodevices.

To now, the combination of different 2D materials has achieved

* Corresponding authors.
E-mail addresses: phamdinhkhang@tdtu.edu.vn (K.D. Pham), buidinhlpt@gmail.com (H.D. Bui), chuongnguyen11@gmail.com (C.V. Nguyen).

https://doi.org/10.1016/j.cplett.2019.136649
Received 15 May 2019; Received in revised form 30 July 2019; Accepted 31 July 2019
Available online 01 August 2019

large achievements in both experiments and theories. First of all, it should be emphasized that there have recently been many common methods that can be used effectively to prepare the vdW-HTSs between 2D materials, such as mechanical exfoliation [20,21], liquid-based techniques [22], and chemical vapor deposition (CVD) [23–25]. For example, Gong and his group suggested a one-step growth approach to preparing the vertical WS_2/MoS_2 vdW-HTS [24]. In addition, such group also reported a two-step CVD method to obtain the $WSe_2/MoSe_2$ HTS [25]. The successful synthesis of 2D materials and their HTSs make them promising materials for the applications in optoelectronics and nanoelectronics. Furthermore, 2D materials and their vdW-HTSs have also attracted interest from theoretical research community [26–39].

More recently, a new type of the alkaline-earth-metal hydroxides family, Portlandite $Ca(OH)_2$, can be obtained from its bulk form [40]. Whereas, a new type of 2D metal dichalcogenide materials, indium selenides (InSe), has also been synthesized experimentally [41]. The electronic and optical properties of both $Ca(OH)_2$ and InSe monolayer are known to be very sensitive to external conditions, including strains and electric field [40,42], making them suitable for future applications in optoelectronics and nanoelectronics. To date, there have been various theoretical and experimental reports on the InSe-based [34,35,43–45] and $Ca(OH)_2$-based [46–49] vdW-HTSs. However, to the best of our knowledge, currently, there is no work that focused on the strain and electric field engineering of band alignment in InSe/$Ca(OH)_2$ vdW-HTS. This motivates us to consider whether InSe and $Ca(OH)_2$ monolayers can form a stable vdW-HTS, and what interesting electronic or optical properties it can provide. Therefore, in this letter, we investigate the band alignment in the combined heterostructure between InSe and $Ca(OH)_2$ monolayers. The effects of strain and electric field on the electronic properties of InSe/$Ca(OH)_2$ vdW-HTS are also considered. Our results reveal that the InSe/$Ca(OH)_2$ vdW-HTS could be a promising material for nanoelectronic devices.

2. Computational methodology

This work was performed from first-principles calculations on the framework of density function theory (DFT). The Quantum Espresso package was selected to calculate all the calculations, including the structural optimization and electronic characteristics calculations of materials. Projector-augmented wave (PAW) method is applied to describe the electron-ion interactions. Whereas, the electron exchange and correlation are treated by the Perdew-Burke-Enzerhof (PBE) functional within the generalized gradient approximation (GGA) formalism. In addition, the effects of vdW interactions, that may exist between two layered materials were also considered by using the Grimme DFT-D2 scheme. A 410 eV of cut-off energy is used and a $(9\times9\times1)$ k-point of Brillouin zone (BZ) is represented. The atomic structure of the vdW-HTS is fully relaxed with the force and total energy convergence of 10^{-4} eV/Å and 10^{-6} eV, respectively. A large vacuum layer thickness of 20 Å along the z direction of vdW-HTS is adopted to eliminate the interaction between two adjacent periodic slabs. Additionally, the calculations were performed using the hybrid HeydScuseriaErnzerhof (HSE) method to check the validity of the results given by the PBE method.

The optical absorption coefficient $\alpha(\omega)$ can be calculated as follows:

$$\alpha(\omega) = \sqrt{2}\,\omega\,[\sqrt{\varepsilon_1^2(\omega) + \varepsilon_2^2(\omega)} - \varepsilon_1(\omega)]^{1/2}, \quad (1)$$

where $\varepsilon_1(\omega)$ and $\varepsilon_2(\omega)$ are the real and imaginary parts of the dielectric function, respectively.

For 2D systems, the carrier mobility can be calculated as follows:

$$\mu_{2D} = \frac{e\tau}{m^*} = \frac{2e\hbar^3 C_{2D}}{3k_B T|m^*|^2 E_1^2} \quad (2)$$

Here, e is electron charge. $T = 273$ K is the temperature. E_1 is the deformation potential, which can be calculated by the shift of the band edges under small strain. m^* represent for the effective mass, that can be calculated by fitting to the band structures at the conduction band minimum and valence band maximum as follows:

$$\frac{1}{m^*} = \frac{1}{\hbar^2}\frac{\partial^2 E}{\partial k^2}. \quad (3)$$

C is the in-plane stiffness, which can be calculated as follows:

$$C_{2D} = \frac{1}{A_0}\frac{\partial^2 E}{\partial \delta^2} \quad (4)$$

Here, E is the total energy of the vdW-HTS. δ is the applied uniaxial strain. A_0 is the area of the considered system.

3. Results and discussion

Before finding an effective way to combine the atomic structures of the combined InSe/$Ca(OH)_2$ vdW-HTS, the geometric structures of the isolated InSe and $Ca(OH)_2$ monolayers are examined. Our DFT calculated lattice parameters of isolated InSe and $Ca(OH)_2$ monolayers, respectively, are 4.06 Å and 3.59 Å, which are in consistent with previous reports [40,50]. Meanwhile, the dynamical stability of InSe and $Ca(OH)_2$ monolayers are also checked by calculating their phonon dispersions. We find that there are no imaginary frequency in the phonon spectrums, which are illustrated in Fig. S1(a-b) (ESI), indicating that both InSe and $Ca(OH)_2$ monolayers are stable. Thus, to make the InSe/$Ca(OH)_2$ vdW-HTS we combine a $(\sqrt{3}\times\sqrt{3})$ InSe supercell with a (2×2) $Ca(OH)_2$ supercell, indicating an overall lattice mismatch of 1.65%. It is noted in previous work that both the InSe and $Ca(OH)_2$ monolayers show good mechanical flexibility because of their layered puckered structures [51,52]. Atomic structure of InSe/$Ca(OH)_2$ vdW-HTS is displayed in Fig. 1. The interlayer distance (D) is obtained to be 2.38 Å when all the atomic positions in InSe/$Ca(OH)_2$ vdW-HTS are fully optimized. In addition, the binding energy of the vdW-HTS is obtained from $E_b = E_{vdW-HTS} - E_I - E_C$, where $E_{vdW-HTS}$, E_I and E_C are respectively the total energies of considered vdW-HTS, isolated InSe and $Ca(OH)_2$ monolayers. The binding energy is calculated to be − 0.47 eV. Both the equilibrium interlayer distance D and E_b imply that such vdW-HTS is energetic stability and is mediated by the weak vdW interactions. Also, the dynamical stability of such InSe/$Ca(OH)_2$ vdW-HTS are checked by calculating its phonon dispersion, as illustrated in Fig. S1(c) (ESI). We find that there is no imaginary frequency in its phonon spectra, confirming the tdynamical stability of such vdW-HTS.

The band structures of isolated InSe and $Ca(OH)_2$ monolayers is illustrated in Fig. 2(a,b), which demonstrates their semiconducting characters. The $Ca(OH)_2$ monolayer displays a direct semiconductor, whereas the InSe monolayer shows an indirect one. The highest occupied energy state of the valence band (HO) and the lowest unoccupied energy state of the conduction band (LU) of $Ca(OH)_2$ monolayer directly locate at the G point, as shown in Fig. 2(a). While the HO of InSe lies along the G–M path and its LU locates at G point. The obtained band gap (E_g) of the $Ca(OH)_2$ and InSe monolayers are 3.68 eV and 1.56 eV, respectively. These values are in good agreement with previous reports [40,53]. Moreover, it should be noted that the PBE method always underestimates the band gap of semiconductors. HSE method is widely used to obtain more accurate band gap value. The band gaps of InSe and $Ca(OH)_2$ monolayers obtained from HSE method are xxx and yyy eV, respectively, as displayed in Fig. S2(a,b) (ESI). Although the PBE method underestimates the band gap, it is still able to predict the correct trend in band gap variation and to properly demonstrate the physical mechanisms, therefore we believe that the results can still be expected to be meaningful. Fig. 2(c) demonstrates the band structure of InSe/$Ca(OH)_2$ vdW-HTS at the equilibrium D. The HO of InSe/$Ca(OH)_2$ vdW-HTS comes from the InSe monolayer, whereas the LU originates from the $Ca(OH)_2$ monolayer. Thus, the InSe/$Ca(OH)_2$ vdW-HTS displays a type-II behavior of heterojunction. It tends to form spatial indirect excitons. The band gap of InSe/$Ca(OH)_2$ vdW-HTS is a direct and its HO and LU locate at the G point. The direct band gap makes the

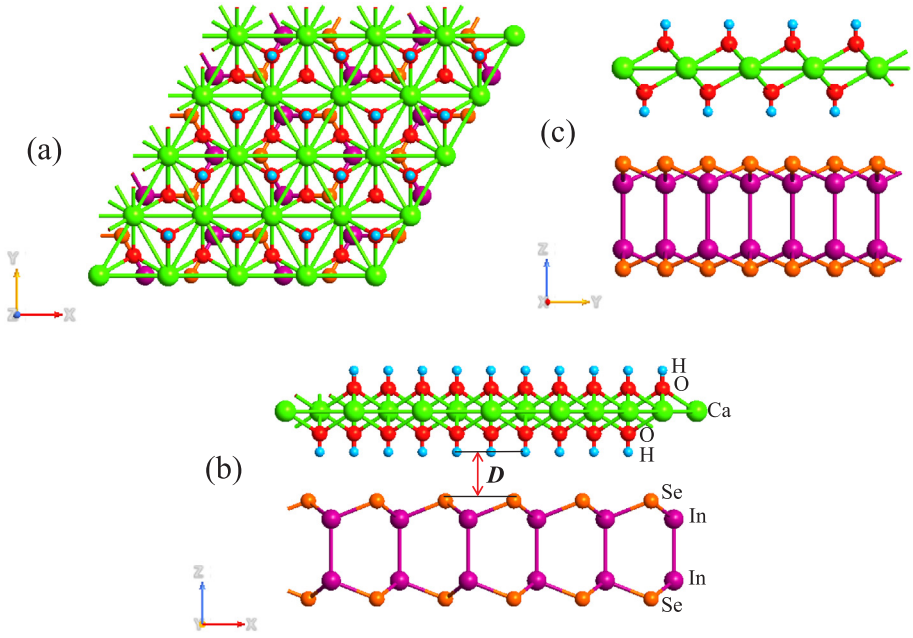

Fig. 1. (a) Top, (b,c) side views of the relaxed atomic structures of the $InSe/Ca(OH)_2$ vdW-HTS at the equilibrium interlayer distance *D*.

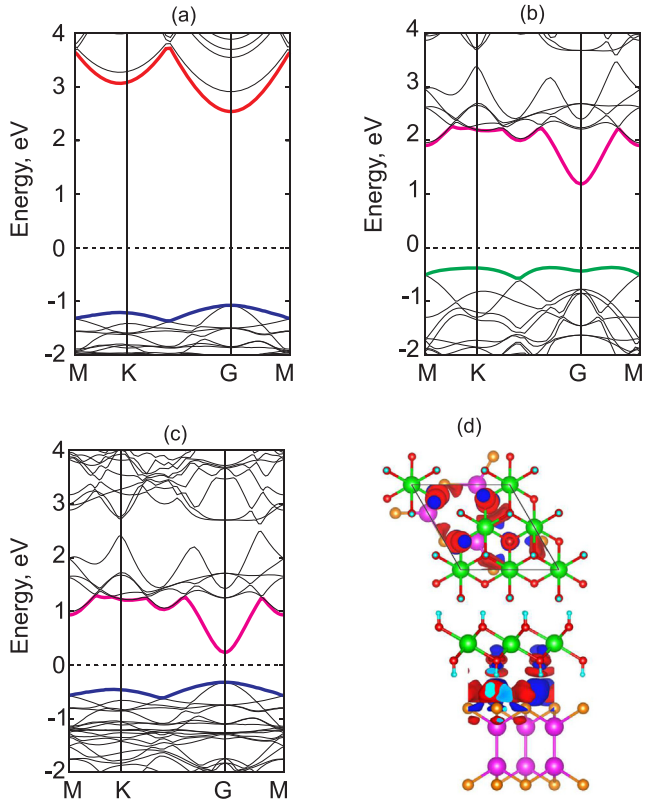

Fig. 2. Calculated band structures of (a) monolayer $Ca(OH)_2$, (b) monolayer InSe, (c) $InSe/Ca(OH)_2$ vdW-HTS. (d) The CDD calculation of the $InSe/Ca(OH)_2$ vdW-HTS along its *z* direction. The red and blue regions mean charge accumulation and depletion, respectively. (For interpretation of the references to colour in this figure legend, the reader is referred to the web version of this article.)

$InSe/Ca(OH)_2$ vdW-HTS suitable for applications in electronic nanodevices [54]. At the equilibrium *D*, the band gap of $InSe/Ca(OH)_2$ vdW-HTS is calculated to be 0.55 eV. Such value is still smaller than that of the isolated $Ca(OH)_2$ and InSe monolayers. It implies that the combination of the InSe and $Ca(OH)_2$ monolayers to form the vdW-HTS tends to a significant decrease in the band gap, which may result from the vacuum energy difference of the monolayers.

In the following, to examine the charge transfer between two monolayers, we calculate the charge density difference (CDD) of the vdW-HTS along its *z* direction as follows: $\Delta\rho = \rho_{vdW-HTS} - \rho_I - \rho_C$, where $\rho_{vdW-HTS}$, ρ_I and ρ_C are the charge densities of considered vdW-HTS, InSe and $Ca(OH)_2$ monolayers, respectively. The CDD calculation is presented in Fig. 2(d). It should be noted that the positive values marked by the red color indicate charge accumulation while negative values marked by the blue color demonstrate charge depletion. We displays in Fig. 3 the optical absorption as a function of photon energies of InSe and $Ca(OH)_2$ monolayers as well as their $InSe/Ca(OH)_2$ vdW-HTS. One can observe from Fig. 3 that the optical absorption in the visible-light region for the $InSe/Ca(OH)_2$ vdW-HTS is enhanced as compared with those of monolayers. Also, the $InSe/Ca(OH)_2$ vdW-HTS has a wide visible light adsorption region with an intensity of 10^5 cm^1. The enhancement of the optical adsorption in the visible-light region is due to the smaller direct band gap of such vdW-HTS. This enhanced

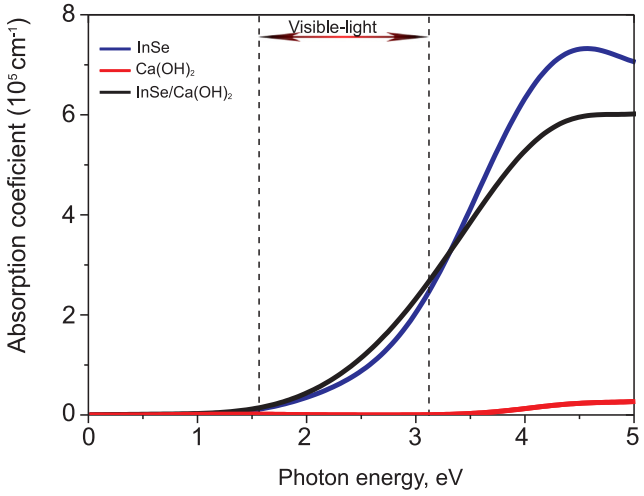

Fig. 3. The optical absorption coefficient $\alpha(\omega)$ of the InSe, $Ca(OH)_2$ monolayer and their $InSe/Ca(OH)_2$ vdW-HTS.

Table 1
Calculated effective mass, deformation potential, in-plane stiffness, and carrier mobility for electron (e) and hole (h) of the isolated InSe and $Ca(OH)_2$ monolayers as well as the InSe/$Ca(OH)_2$ vdW-HTS.

Carrier type	Materials	m^*/m_0	E_1 [eV]	C_{2D} [N/m]	μ [cm^2/Vs]
Electron	InSe	0.210	5.14	54.24	1629
	$Ca(OH)_2$	0.604	5.34	60.20	201
	InSe/$Ca(OH)_2$	0.24	4.12	105.30	3760
Hole	InSe	2.063	1.84	54.24	131
	$Ca(OH)_2$	0.446	4.32	60.20	565
	InSe/$Ca(OH)_2$	0.573	3.73	105.30	1146

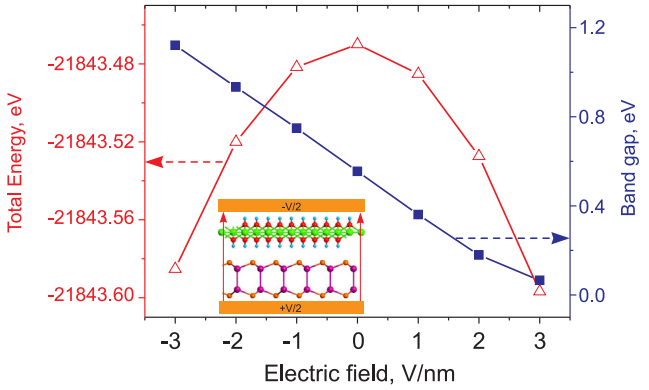

Fig. 4. The variation of the total energy and band gap of the InSe/$Ca(OH)_2$ vdW-HTS as a function of electric field, applying along the *z* direction.

optical absorption of such vdW-HTS is more suitable for in photoelectronic devices.

The carrier mobility of the InSe, $Ca(OH)_2$ monolayers and their InSe/$Ca(OH)_2$ vdW-HTS at room temperature is listed in Table 1. One can observe that the carrier mobility in InSe/$Ca(OH)_2$ vdW-HTS is increased as compared with InSe and $Ca(OH)_2$ monolayers, with electron mobility increased to 3760 cm^2/Vs and 1164 cm^2/VS for hole. The electron mobility of the InSe/$Ca(OH)_2$ vdW-HTS nearly threefold increased in comparison to that of InSe monolayer. Whereas, the hole mobility of such vdW-HTS increases by two times in comparison with that of $Ca(OH)_2$ monolayer. Such increase shows its great potential application in next-generation high-performance nanoelectronic devices.

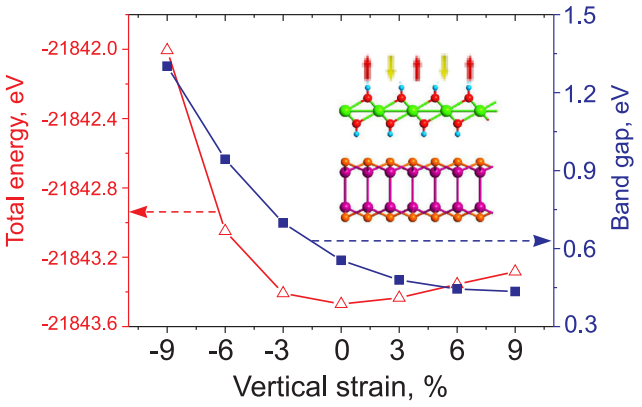

Fig. 6. The dependence of the total energy and band gap of the InSe/$Ca(OH)_2$ vdW-HTS as a function of the vertical strain ε.

Now, an interesting phenomenon that should be considered is whether the band gap of such InSe/$Ca(OH)_2$ vdW-HTS can be modulated by applying electric field ($E_\perp$) or by changing the interlayer distance *D*? We apply the $E_\perp$ perpendicularly to the vdW-HTS surface, i.e., along its *z* direction. The variation of the total energy and the band gap of the InSe/$Ca(OH)_2$ vdW-HTS as a function of the $E_\perp$ is illustrated in

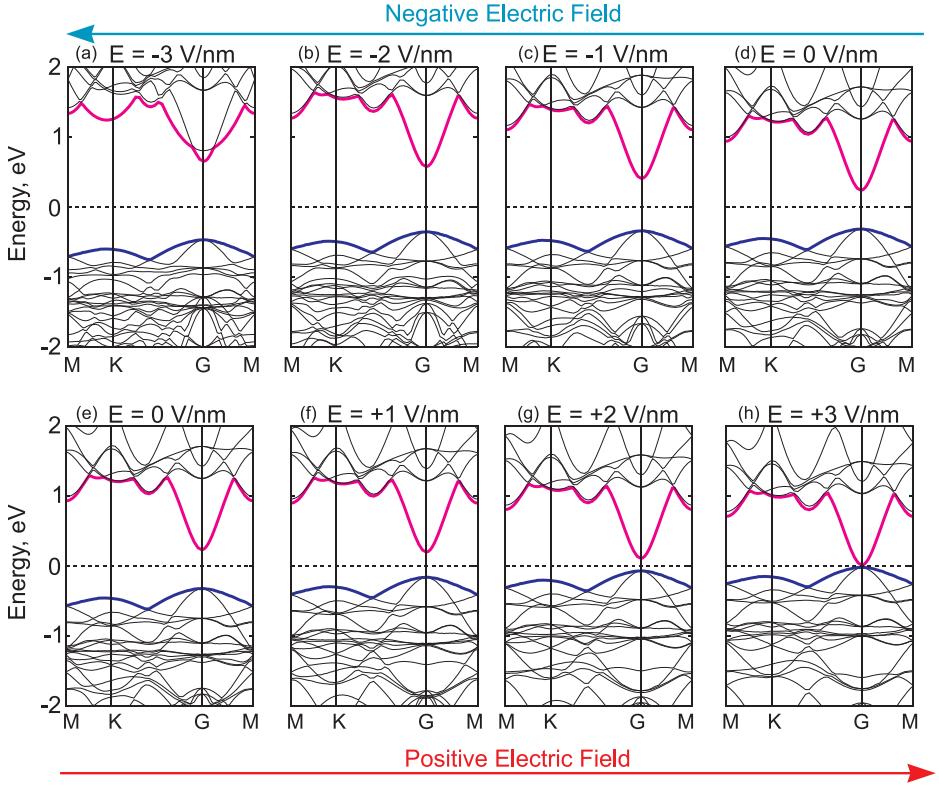

Fig. 5. Calculated band structures of the InSe/$Ca(OH)_2$ vdW-HTS under negative $E_\perp$: (a) $E_\perp = -3$ V/nm, (b) $E_\perp = -2$ V/nm, (c) $E_\perp = -1$ V/nm, (d) $E_\perp = 0$ V/nm and under positive $E_\perp$: (e) $E_\perp = 0$ V/nm, (f) $E_\perp = +1$ V/nm, (g) $E_\perp = +2$ V/nm, (h) $E_\perp = +3$ V/nm.

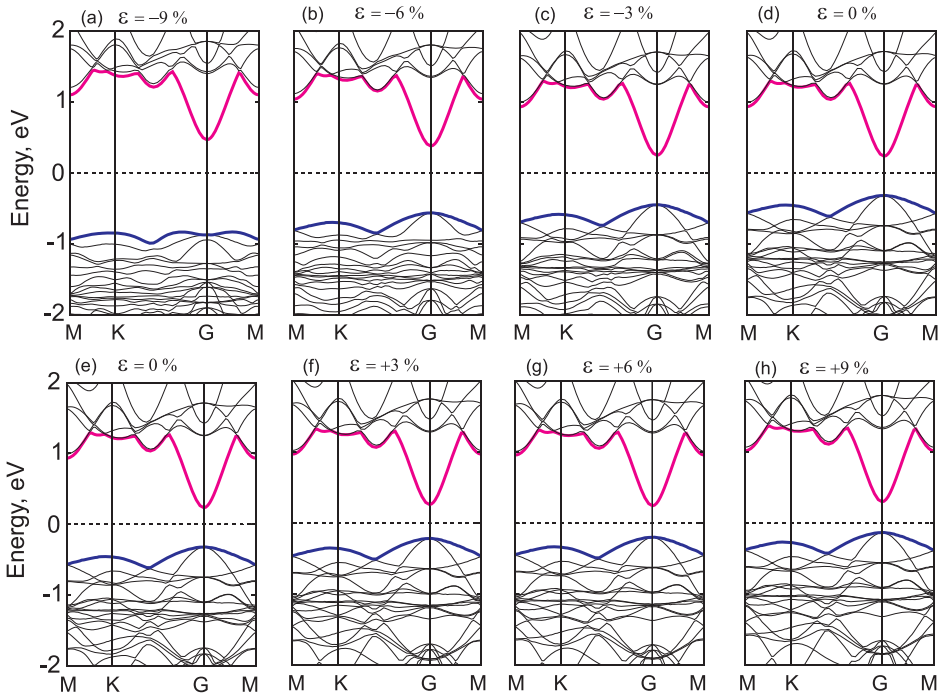

Fig. 7. Calculated band structures of the InSe/$Ca(OH)_2$ vdW-HTS under different vertical strain ε.

Fig. 4. We find that an applied $E_\perp$ results in a decrease in the total energy of the vdW-HTS. It indicates that the system is much more energetic stable. When a negative $E_\perp$ is applied, we observe a linear increase in the band gap of the InSe/$Ca(OH)_2$ vdW-HTS. The value of the band gap increases from 0.55 eV to 0.75 eV and to 1.12 eV when the strength of an applied negative $E_\perp$ varied from 0 V/nm to − 1 V/nm and then to − 3 V/nm, respectively. Quite the contrary, we can see that the band gap of the vdW-HTS decreases with increasing the strength of an applied positive $E_\perp$. It decreases from 0.55 eV at $E_\perp$ = 0 V/nm to nearly zero eV at $E_\perp$ = + 3 V/nm. It indicates that the semiconductor to metal transition can be achieved in the InSe/$Ca(OH)_2$ vdW-HTS by applying a large positive $E_\perp$ of + 3 V/nm.

Fig. 5 presents the band structures of the InSe/$Ca(OH)_2$ vdW-HTS under different strengths of applied negative and positive $E_\perp$. We observe that an applied negative $E_\perp$ leads to an increase in the band gap of such vdW-HTS. It can be seen that by applying a negative $E_\perp$ both the HO and LU of the vdW-HTS move away from the Fermi level, resulting in a dramatic increase in its band gap. Whereas, by applying a positive $E_\perp$, its HO and LU move towards the Fermi level, leading a decrease in a gap size of vdW-HTS. The nature of the change in the band gap size of such vdW-HTS may relate to the built-in electric field, that is occurred between two monolayers due to their difference in work function. Our calculated work function for InSe and $Ca(OH)_2$ monolayers are 5.67 eV and 4.79 eV, respectively. It also indicates that the charge transfer points from the InSe layer to the $Ca(OH)_2$ layer. Under a positive $E_\perp$ of + 3 V/nm, both the HO and HU of the vdW-HTS cross the Fermi level. In this case, the vdW-HTS has a metallic character, demonstrating a transition from semiconductor to metal under a large applied positive $E_\perp$ of + 3 V/nm.

Now we turn to consider the vertical strain engineering of the electronic properties of the InSe/$Ca(OH)_2$ vdW-HTS. This strain was applied by decreasing and increasing the D between the two monolayers, as shown in Fig. 6. The vertical strain is defined as $\varepsilon = (D' - D)/D$, where D' is the strained interlayer distance. The InSe/$Ca(OH)_2$ vdW-HTS has a lowest total energy at ε = 0%. The band gap of the InSe/$Ca(OH)_2$ vdW-HTS decrease with increasing the vertical strain from − 9% to + 9%. It should be noted that the InSe/$Ca(OH)_2$ vdW-HTS is dynamical stable at the vertical strain of + 9%, as displayed in Fig. S3. With increasing the vertical strain from − 9% to + 9%, the band gap of the vdW-HTS decreases from 1.30 eV to 0.43 eV, respectively. To clearly understand the change in the band gap values of the vdW-HTS under the vertical strains, we further calculate its band structures under different values of the vertical compressive and tensile strains, as shown in Fig. 7. It can be observed that the vdW-HTS is a direct semiconductor at the equilibrium state of D = 2.322 Å. When the D is compressed from 0% down to − 3% and then to − 9%, the band gap of the vdW-HTS increases from 0.55 eV down to 0.70 eV and then to 1.30 eV, respectively. The reason for this reduction is related to the change in the position of the LU and HO of the vdW-HTS. When the D is compressed, the position of both the LU and HO of the vdW-HTS is moved away from its Fermi level. It leads to an increase in the band gap of the vdW-HTS, as discussed above. Moreover, under the compressive vertical strain of − 9%, we find a transition from direct band gap to an indirect one, as illustrated in Fig. 7(a). It should be noted that the indirect band gap semiconductor of such vdW-HTS has low absorption coefficient, which has limited its potential applications in optoelectronics devices [55,56]. The LU of the vdW-HTS locates at the G-point, whereas its HO moves from the G-point to the G–M path. On the other hand, when increasing the vertical strain from 0% to + 9%, both the HO and LU of the vdW-HTS move towards its Fermi level. It results in a decrease in the band gap of the InSe/$Ca(OH)_2$ vdW-HTS, as illustrated in Fig. 6. Thus, we can conclude that the band gap of the InSe/$Ca(OH)_2$ vdW-HTS can be engineered by the vertical strains, therefore, it can be used as a component of electronic nanodevices.

4. Conclusion

In summary, we have investigated the structural and electronic properties of the combination between InSe and $Ca(OH)_2$ to form the InSe/$Ca(OH)_2$ vdW-HTS using DFT calculations. The results indicate that such vdW-HTS is energetic stability and is mediated by the weak vdW interactions. The InSe/$Ca(OH)_2$ vdW-HTS possesses a type-II semiconductor with a direct band gap of 0.55 eV. Furthermore, it implies that the combination of the InSe and $Ca(OH)_2$ monolayers to form the vdW-HTS tends to a significant decrease in the band gap, which may result from the vacuum energy difference of the monolayers.

Furthermore, the band gap and band alignment in the InSe/$Ca(OH)_2$ vdW-HTS can be also engineered by strain and electric field, it, therefore, can be used as a component of optoelectronic nanodevices. The semiconductor-to-metal and direct-to-indirect transitions can also emerge, which make InSe/$Ca(OH)_2$ vdW-HTS promising material for electronic nanodevices.

Declaration of Competing Interest

The authors declare that they have no known competing financial interests or personal relationships that could have appeared to influence the work reported in this paper.

Acknowledgements

This research is funded by the Vietnam National Foundation for Science and Technology Development (NAFOSTED) under Grant No. 103.01-2017.309. B. Amin acknowledges support from the Higher Education Commission of Pakistan (HEC) under Project No. 5727/261 KPK/NRPU/R&D/HEC2016.

Appendix A. Supplementary material

Supplementary data associated with this article can be found, in the online version, at https://doi.org/10.1016/j.cplett.2019.136649.

References

[1] K.S. Novoselov, et al., Electric field effect in atomically thin carbon films, Science 306 (5696) (2004) 666–669.
[2] Q.H. Wang, K. Kalantar-Zadeh, A. Kis, J.N. Coleman, M.S. Strano, Electronics and optoelectronics of two-dimensional transition metal dichalcogenides, Nat. Nanotechnol. 7 (11) (2012) 699.
[3] J.N. Coleman, et al., Two-dimensional nanosheets produced by liquid exfoliation of layered materials, Science 331 (6017) (2011) 568–571.
[4] M. Chhowalla, H.S. Shin, G. Eda, L.-J. Li, K.P. Loh, H. Zhang, The chemistry of two-dimensional layered transition metal dichalcogenide nanosheets, Nat. Chem. 5 (4) (2013) 263.
[5] G.R. Bhimanapati, et al., Recent advances in two-dimensional materials beyond graphene, ACS Nano 9 (12) (2015) 11509–11539.
[6] M. Xu, T. Liang, M. Shi, H. Chen, Graphene-like two-dimensional materials, Chem. Rev. 113 (5) (2013) 3766–3798.
[7] S.Z. Butler, et al., Progress, challenges, and opportunities in two-dimensional materials beyond graphene, ACS Nano 7 (4) (2013) 2898–2926.
[8] H. Liu, A.T. Neal, Z. Zhu, Z. Luo, X. Xu, D. Tománek, P.D. Ye, Phosphorene: an unexplored 2D semiconductor with a high hole mobility, ACS Nano 8 (4) (2014) 4033–4041.
[9] D.J. Late, et al., GaS and GaSe ultrathin layer transistors, Adv. Mater. 24 (26) (2012) 3549–3554.
[10] M. Yarmohammadi, The effects of strain on dc transverse and spin-valley hall conductivity of ferromagnetic MoS_2 and silicene, J. Magn. Magn. Mater. 426 (2017) 621–628.
[11] B. Hoi, M. Yarmohammadi, Combined effect of the perpendicular magnetic field and dilute charged impurity on the electronic phase of bilayer AA-stacked hydrogenated graphene, Phys. Lett. A 382 (45) (2018) 3298–3305.
[12] B. Hoi, M. Yarmohammadi, M. Davoudiniya, Coherent control of the route of magnetic phases in quasi-1D armchair graphene nanoribbons via doping in the presence of electronic correlations, Solid State Commun. 271 (2018) 21–28.
[13] M. Yarmohammadi, Impurity doping effects on the orbital thermodynamic properties of hydrogenated graphene, graphane, in Harrison model, Phys. Lett. A 380 (48) (2016) 4062–4069.
[14] M. Yarmohammadi, Perturbation tuning of plasmon modes in semiconductor armchair nanoribbons, Phys. Rev. B 98 (2018) 155424.
[15] P.D. Khang, M. Davoudiniya, L.T.T. Phuong, T.C. Phong, M. Yarmohammadi, Optical interband transitions in strained phosphorene, Phys. Chem. Chem. Phys. 21 (2019) 15133–15141.
[16] D.Q. Khoa, M. Davoudiniya, B.D. Hoi, M. Yarmohammadi, Strain engineering of optical activity in phosphorene, RSC Adv. 9 (2019) 19006–19015.
[17] H. Bui, L.T.T. Phuong, M. Yarmohammadi, On the influence of dilute charged impurity and perpendicular electric field on the electronic phase of phosphorene: band gap engineering, Europhys. Lett. 124 (2) (2018) 27001.
[18] P.T.T. Le, M. Yarmohammadi, Tuning thermoelectric transport in phosphorene through a perpendicular magnetic field, Chem. Phys. 519 (2019) 1–5.
[19] P.T.T. Le, M. Davoudiniya, M. Yarmohammadi, Interplay of orbital hopping and perpendicular magnetic field in anisotropic phase transitions for Bernal bilayer graphene and hexagonal boron-nitride, Phys. Chem. Chem. Phys. 21 (1) (2019) 238–245.
[20] Y. Liu, N.O. Weiss, X. Duan, H. Cheng, Y. Huang, X. Duan, Van der waals heterostructures and devices, Nat. Rev. Mater. 1 (9) (2016) 16042.
[21] J. He, N. Kumar, M.Z. Bellus, H.-Y. Chiu, D. He, Y. Wang, H. Zhao, Electron transfer and coupling in graphene–tungsten disulfide van der waals heterostructures, Nat. Commun. 5 (2014) 5622.
[22] V. Nicolosi, M. Chhowalla, M.G. Kanatzidis, M.S. Strano, J.N. Coleman, Liquid exfoliation of layered materials, Science 340 (6139) (2013) 1226419.
[23] Z. Cai, B. Liu, X. Zou, H.-M. Cheng, Chemical vapor deposition growth and applications of two-dimensional materials and their heterostructures, Chem. Rev. 118 (13) (2018) 6091–6133.
[24] Y. Gong, et al., Vertical and in-plane heterostructures from WS_2/MoS_2 monolayers, Nat. Mater. 13 (12) (2014) 1135.
[25] Y. Gong, et al., Two-step growth of two-dimensional WSe_2/$MoSe_2$ heterostructures, Nano Lett. 15 (9) (2015) 6135–6141.
[26] W. Wei, Y. Dai, C. Niu, X. Li, Y. Ma, B. Huang, Electronic properties of two-dimensional van der waals GaS/GaSe heterostructures, J. Mater. Chem. C 3 (43) (2015) 11548–11554.
[27] Q. Peng, Z. Wang, B. Sa, B. Wu, Z. Sun, Electronic structures and enhanced optical properties of blue phosphorene/transition metal dichalcogenides van der waals heterostructures, Sci. Rep. 6 (2016) 31994.
[28] M. Sun, J.-P. Chou, J. Yu, W. Tang, Electronic properties of blue phosphorene/graphene and blue phosphorene/graphene-like gallium nitride heterostructures, Phys. Chem. Chem. Phys. 19 (2017) 17324–17330.
[29] M. Sun, J.-P. Chou, Q. Ren, Y. Zhao, J. Yu, W. Tang, Tunable schottky barrier in van der waals heterostructures of graphene and g-GaN, Appl. Phys. Lett. 110 (2017) 173105.
[30] M. Sun, J.-P. Chou, J. Yu, W. Tang, Effects of structural imperfection on the electronic properties of graphene/WSe_2 heterostructures, J. Mater. Chem. C 5 (39) (2017) 10383–10390.
[31] Z. Ben Aziza, et al., Van der waals epitaxy of GaSe/Graphene heterostructure: electronic and interfacial properties, ACS Nano 10 (10) (2016) 9679–9686.
[32] C. Si, Z. Lin, J. Zhou, Z. Sun, Controllable Schottky barrier in GaSe/graphene heterostructure: the role of interface dipole, 2D Mater. 4 (1) (2016) 015027.
[33] H. Din, M. Idrees, T.A. Alrebdi, C.V. Nguyen, B. Amin, Electric field tunable electronic properties of p-ZnO and Si-ZnO van der Waals heterostructures, Comput. Mater. Sci. 164 (2019) 166–170.
[34] C.V. Nguyen, H. Bui, T.D. Nguyen, K.D. Pham, Controlling electronic properties of PtS_2/InSe van der Waals heterostructure via external electric field and vertical strain, Chem. Phys. Lett. 724 (2019) 1–7.
[35] K.D. Pham, et al., Vertical strain and electric field tunable electronic properties of type-II band alignment C_2N/InSe van der Waals heterostructure, Chem. Phys. Lett. 716 (2019) 155–161.
[36] K. Tang, W. Qi, Y. Li, T. Wang, Electronic properties of van der waals heterostructure of black phosphorus and MoS_2, J. Phys. Chem. C 122 (12) (2018) 7027–7032.
[37] L. Peng, Y. Cui, L. Sun, J. Du, S. Wang, S. Zhang, Y. Huang, Dipole controlled schottky barrier in the blue-phosphorene-phase of GeSe based van der waals heterostructures, Nanoscale Horiz. 4 (2) (2019) 480–489.
[38] J. Shi, et al., Tuning the electronic structure of GeC/WS_2 van der Waals heterostructure by electric field and strain: A first principles study, Comput. Mater. Sci. 160 (2019) 301–308.
[39] W. Zhang, et al., Interlayer coupling and external electric field tunable electronic properties of a 2D type-I α-tellurene/MoS2 heterostructure, J. Mater. Chem. C 6 (38) (2018) 10256–10262.
[40] Y. Aierken, et al., Portlandite crystal: bulk, bilayer, and monolayer structures, Phys. Rev. B 91 (24) (2015) 245413.
[41] W. Huang, L. Gan, H. Li, Y. Ma, T. Zhai, 2D layered group IIIA metal chalcogenides: synthesis, properties and applications in electronics and optoelectronics, CrystEngComm 18 (22) (2016) 3968–3984.
[42] H. Jin, J. Li, Y. Dai, Y. Wei, Engineering the electronic and optoelectronic properties of InX (X = S, Se, Te) monolayers via strain, Phys. Chem. Chem. Phys. 19 (6) (2017) 4855–4860.
[43] Y. Ding, et al., Enhancement of hole mobility in InSe monolayer via an InSe and black phosphorus heterostructure, Nanoscale 9 (38) (2017) 14682–14689.
[44] Y. Ding, et al., Electric field modulation of electronic structures in inse and black phosphorus heterostructure, Solid State Commun. 269 (2018) 112–117.
[45] J. Zhang, X. Lang, Y. Zhu, Q. Jiang, Strain tuned InSe/MoS_2 bilayer van der waals heterostructures for photovoltaics or photocatalysis, Phys. Chem. Chem. Phys. 20 (26) (2018) 17574–17582.
[46] X.-H. Li, B.-J. Wang, X.-L. Cai, W.-Y. Yu, L.-W. Zhang, G.-D. Wang, S.-H. Ke, Arsenene/$Ca(OH)_2$ van der Waals heterostructure: strain tunable electronic and photocatalytic properties, RSC Adv. 7 (70) (2017) 44394–44400.
[47] C. Bacaksiz, A. Dominguez, A. Rubio, R.T. Senger, H. Sahin, h-AlN-$Mg(OH)_2$ van der Waals bilayer heterostructure: tuning the excitonic characteristics, Phys. Rev. B 95 (7) (2017) 075423.
[48] Q. Gao, C. Xia, W. Xiong, J. Du, T. Wang, Z. Wei, J. Li, Type-I $Ca(OH)_2$/α-$MoTe_2$ vdW heterostructure for ultraviolet optoelectronic device applications: electric field effects, J. Mater. Chem. C 5 (47) (2017) 12629–12634.
[49] E. Torun, H. Sahin, F. Peeters, Optical properties of GaS-$Ca(OH)_2$ bilayer heterostructure, Phys. Rev. B 93 (7) (2016) 075111.
[50] L. Debbichi, O. Eriksson, S. Lebègue, Two-dimensional indium selenides compounds: an ab initio study, J. Phys. Chem. Lett. 6 (15) (2015) 3098–3103.
[51] T. Hu, J. Zhou, J. Dong, Strain induced new phase and indirect–direct band gap transition of monolayer InSe, Phys. Chem. Chem. Phys. 19 (32) (2017) 21722–21728.
[52] C. Xia, W. Xiong, J. Du, T. Wang, Z. Wei, J. Li, Robust electronic and mechanical

properties to layer number in 2D wide-gap $X(OH)_2$ (X= Mg, Ca), J. Phys. D: Appl. Phys. 51 (1) (2017) 015107.
[53] G. Mudd, et al., The direct-to-indirect band gap crossover in two-dimensional van der waals indium selenide crystals, Sci. Rep. 6 (2016) 39619.
[54] B. Yang, et al., Lead-free direct band gap double-perovskite nanocrystals with bright dual-color emission, J. Am. Chem. Soc. 140 (49) (2018) 17001–17006.
[55] B. Yang, et al., Lead-free, air-stable all-inorganic cesium bismuth halide perovskite nanocrystals, Angew. Chem. Int. Ed. 56 (41) (2017) 12471–12475.
[56] B. Yang, et al., Lead-free silver-bismuth halide double perovskite nanocrystals, Angew. Chem. 130 (19) (2018) 5457–5461.